ISSN: 2998-8713

Research Article

Journal of data Analytics and Engineering Decision Making

Effect of Chromium Coating deposited by magnetron sputtering on mechanical and microstructural behaviour of Superni -718

Shahnaz Bashir Bhat*, Mukund Dutt Sharma and Atikur Rahman

Department of Metallurgical and Materials Engineering, National Institute of Technology Srinagar, India

***Corresponding Author**
Shahnaz Bashir Bhat, Department of Metallurgical and Materials Engineering, National Institute of Technology Srinagar, India.

Submitted: 2025, Jul 18; **Accepted:** 2025, Aug 11; **Published:** 2025, Aug 21

Citation: Bhat, B. S., Sharma, D. M., Rahman, A. (2025). Effect of Chromium Coating deposited by magnetron sputtering on mechanical and microstructural behaviour of Superni -718. *J Data Analytic Eng Decision Making, 2*(2), 01-13.

Abstract

For high-temperature applications, super alloys, especially those based on nickel, are recommended because of their superior mechanical strength at high service temperatures. To overcome such constraints, the coating has been done to enhance the mechanical properties of the substrate. This work investigated samples coated with Chromium coating using DC magnetron sputtering. The surface morphology and composition were evaluated using EDS and FE-SEM, XRD revealed different phases both on substrate and chromium coated sample, and atomic force microscopy revealed depth of indent. The microstructure showed that coated specimens exhibited high substrate adherence and little micros scaling. The hardness and elastic modulus of chromium coated sample was performed using Nano indentation based on Oliver and Pharr model and loads ranging from 200μN-1000μN and results exhibited that there is a 52% increase in hardness on every load as well as the modulus of elasticity has increased to 21% and to check the coating adherence three Nano scratches were performed on chromium coated sample at a load of 2000μN.

Keywords: EDS.FESEM, XRD, AFM, Nano Indentation, Magnetron Sputtering

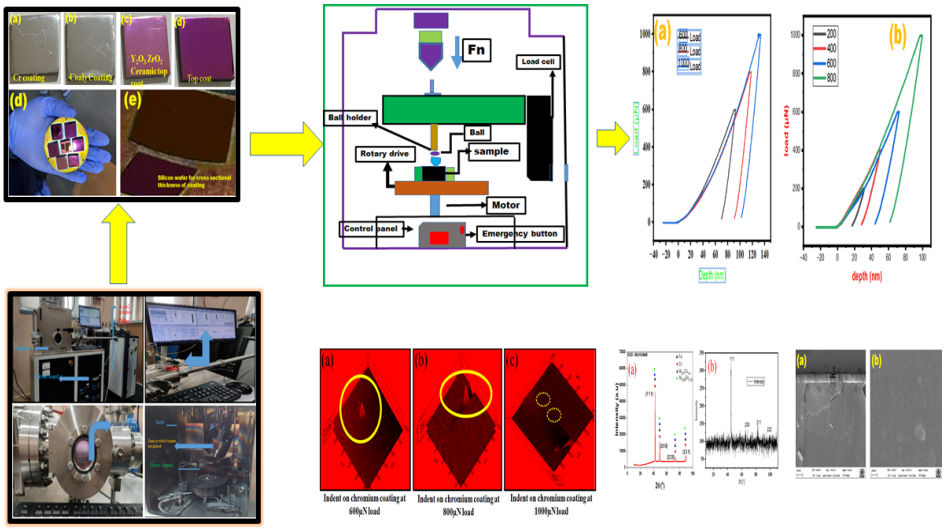

Graphical Abstract for Deposition of Chromium Coating on Super-718 Substrate

1. Introduction

Superni-718 is a nickel-based super alloy known for its excellent mechanical strength, corrosion resistance, and high-temperature performance, making it suitable for applications in aerospace, gas turbines, and nuclear reactors. It exhibits outstanding weldability and resistance to creep and oxidation, primarily due to the presence of elements such as chromium, molybdenum, and niobium, which contribute to its superior mechanical properties [1]. The alloy undergoes precipitation hardening, where γ′ (Ni_3 (Al, Ti)) and γ″ (Ni_3Nb) phases enhance its strength and stability at elevated temperatures [2]. Coatings have been used in several applications to improve contact performance and increase the service life of components. Multilayer coatings produced using the sputtering method can have homogenous layers and allow fine-tuning of the properties of the final coating by varying the individual layer thickness at the nanoscale [3]. Recent studies have explored the application of protective coatings like chromium to improve its wear and oxidation resistance as well mechanical properties, further extending its industrial usability [4].It has been crucial for numerous sectors to achieve high temperatures [1]. Industrial materials are exposed to various applications in which they function in harsh temperatures, pressure, and corrosive environments; as a result, they are susceptible to oxidation, corrosion, and erosion. Thus, their surfaces must be modified to shield these components from deterioration [1-7]. The extensive body of technical literature and surveys demonstrates that industry inefficiency stems from deterioration, as over half of India's electricity uses coal as the primary fuel. A significant proportion of ash, a non-combustible component, and a variable amount of sulfur can be found in coal, a combustible black sedimentary rock. About 15% of ash contains hard quartz, which makes coal more prone to erosion [2-3]. It is crucial to comprehend hot corrosion and high-temperature oxidation since they are significant contributors to the failure of hot section components due to high-temperature degradation. The issues above make it evident that hard coatings must be deposited for a dense, sticky film to form around the substrate, and physical vapor deposition is often the best method for combining material qualities. The most obvious point for investigation is the nanostructured chromium coating since it exhibits exceptional hardness, corrosion, and oxidation resistance at extreme temperatures. The current study examines the erosion-corrosion performance of Superni 718 (Inconel718), a nickel-based superalloy [6]. A commonly used technique to ascertain a material's hardness and elastic characteristics is to indent it to different depths. A more thorough examination of the mechanical characteristics of thin films and materials at the sub-micron and nanoscale levels is now possible thanks to recent significant advancements in developing Nanoindentation techniques [8-11]. Even though the Nanoindentation unloading curve is frequently nonlinear, Oliver and Pharr presented a method for calculating elastic moduli by evaluating the slope of the curve. With the help of their process, one can determine the contact area at the peak load by calculating the appropriate depth and accounting for the indenter's shape. Oliver and Pharr [12] proposed the most widely used method for measuring elastic moduli and hardness through Nanoindentation. As the indentation is frequently impacted by both the film and the underlying substrate, separating the actual properties of the thin film from the data has long been a challenge. When the thin film is thick enough to be handled like a bulk material, its properties are frequently measured using the Oliver and Pharr (1992) approach. [10]. A novel mechanical behavior of crystalline materials has begun to appear at the microscale. For example, the closely spaced nanoparticles can incorporate evenly distributed stress into amorphous nanostructured materials. When working with very thin films, the substrate significantly affects the indentation results at all practical depths. It is imperative to meticulously consider the substrate's influence to determine the thin film's distinct characteristics precisely. The Oliver and Pharr method is frequently employed when selecting the hardness and Young's Modulus in certain situations. Joslin and Oliver proposed [9] a technique that helps prevent the requirement to compute the contact area, which can occasionally cause mistakes in the findings because of material accumulating or sinking into the indentation [8]. One area where Nano indentation is applied is the investigation of the mechanical properties of ceramic coatings, thermal barrier coating or bond coating under various environmental conditions, such as high temperature and humidity. Analysing the effects of

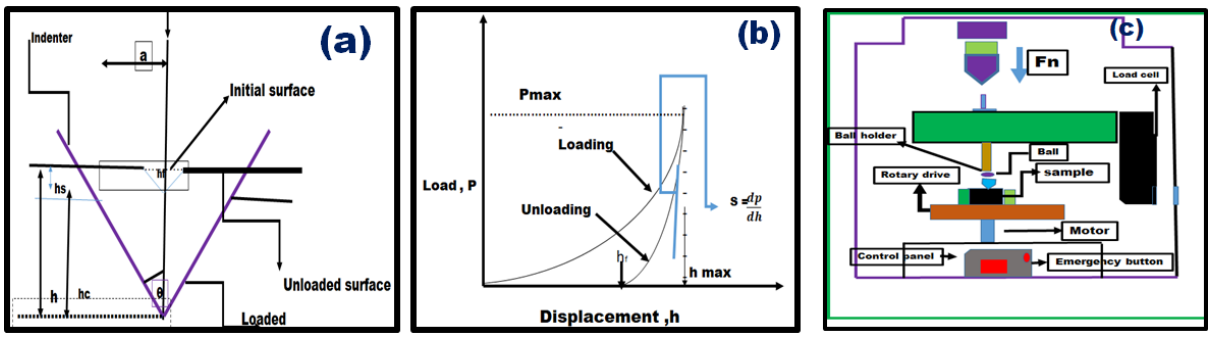

Figure 1: (a) Deformation Pattern of Elastic Plastic Specimen During and After Indentation (b) Standard Load vs Displacement (c) Systematic of Indentation Machine

Different manufacturing settings on the mechanical properties of ceramic coatings is another use for Nano indentation. The Nano indentation hardness is calculated as the indentation load (P) divided by the predicted contact area (A) of the indentation method. It is the maximum average pressure that a substance can withstand when under load. From the load-displacement curve, the hardness at maximum load can be obtained as

$$H = \frac{Pmax}{A} \quad (1)$$

The typical load versus displacement curve and the pattern of deformation of an elastic-plastic sample both before and after indentation (a) are depicted in Figure. 1(a). Figure. 1(b) uses the symbol h_{max} to represent the displacement under P_{max}, the maximum load. When under stress, the contact depth abbreviated as hc maintains the space between the sample and the indenter. The final displacement after total unloading is hf. S represents the stiffness of the first unloading contact [13-15].

The indented sample's elastic modulus can be calculated using the stiffness of the initial unloading contact.

$$S = \frac{dp}{dh} \quad (2)$$

Using the contact stiffness, the reduced modulus (Er) can be calculated

$$E_r = \frac{1}{\beta}\frac{\sqrt{\pi}}{2}\frac{S}{\sqrt{A}} \quad (3)$$

For the Berkovich indenter, the correction factor β is 1.034, and A is the actual contact area. The relationship between A *and* the contact depth (hc) is as follows:

$$A = 24.5\ h_c^2 \quad (4)$$

Using the equation
As the penetration depth h increases, the measured E_r value varies when the film modulus Ei deviates from the substrate E_s. The lowered Young's modulus can be written as follows, assuming that the substrate and thin film's Young's moduli stay similar:

$$\frac{1}{Er} = \frac{1-\nu^2}{E} + \frac{1-\nu i^2}{Ei} \quad (5)$$

Where E is the elastic modulus of the coating.

ν is the poison ratio of the test material

Ei elastic modulus of indenter Ei =1141 GPa

νi_{is} the poison ratio indenter νi = 0.07
To determine the area function, series of indents at various constant depth (varying normal loads) are performed in a sample of know elastic modulus (typically finished quartz) and the constant area (A) is calculated. A plot of the calculated area as a function of contact depth is created and triboscan software fits the A versus hc curve to the sixth order polynomial and the equation is enumerated below

$$A = C_0hc^2 + C_1hc + C_2hc^{1/2} + C_3hc^{1/4} + C_4hc_{1/8} + C_5hc^{1/16} \quad (6)$$

Thus, a basic understanding of the mechanical characteristics, deformation behaviour, and generation of substrate defects of ultra-thin amorphous oxide coatings is crucial for surface engineering. These findings advance our knowledge of the surface-related origins of wear and deformations. They might someday make it possible to create new, longer-lasting, higher-quality oxygen-free structures and technologies [16-17]. By combining ceramics with different thermal expansion coefficients, laminated structures with the goal of producing compressive residual stresses at the surface can be created, improving the surface hardness of materials without causing phase change problems [18]. Material adhesion issues are a major cause of failure in a lot of packing methods, Issues like buckling, cracking, void formation, and film delamination will arise when materials like metal-to-metal, metal-to-ceramic, metal-to-polymer, or polymer-to-ceramic are linked [19-22]. In order to increase wear resistance, micro hardness, oxidation resistance, and corrosion resistance, surface coating technique applies a layer of hard materials to the substrate surface. Several surface coating methods, including direct-current magnetron sputtering (DCMS), are used to enhance the surface characteristics of these components [23-24] radio-frequency magnetron Sputtering (RFMS) [25-26] HiPIMS, or high-power impulse magnetron sputtering [27-31] and EBPVD, or electron beam physical vapour deposition, are employed [32-33] . When electron beam deposition is used, the coating material ionises, evaporates, and is subsequently deposited on the substrate inside the chamber. The thin films produced by the EBPVD method are stress-resistant and have a columnar microstructure. The connection between performance and deposition processes has been supported by numerous investigations. Additionally, examined are the crystallographic texture and microstructure of EBPVD TBC at different vapour deposition angles [34]. Many coatings and structural characteristics can form on a large rotating plate. Because of uniform deposition, the coatings are made up of dense, fine grain that is stationary [35].

2. Experiment

The ni-based super alloy was procured from the mastermind in the form of rolled sheets in different dimensions. The chemical composition of the superalloy sample was examined. The specimens measuring approximately 20 mm in length, 20mm in breadth, and 5 mm in thickness were prepared using an EDM cutting machine. The specimens were polished using different emery paper grades ranging from 220 to fine emery paper up to 3000 grades, alumina powder followed by diamond paste were used to get a good polished surface and chromium target having Chromium (99% pure and 58.5 mm diameter and 5mm thickness)

Midhani Grade	Fe	Ni	Cr	Ti	Al	Mo	Mn	Si	Co	Nb	P	C	S
super-718	19.8	BAL	17.6	0.96	0.53	3.23	0.02	0.03	0.01	4.91	0.005	0.02	0.007

Table 1: Chemical Composition of The Super Alloy (super-718) Used in the Study Using Raman Spectroscopy

FESEM	Field Emission Scanning Electron Spectroscopy
XRD	X-Ray Diffraction
EDS	Energy Dispersive Spectroscopy
AFM	Atomic force microscope
TBC	Thermal barrier coating
Cr	Chromium

Table 2: Symbols and Abbreviations Used

2.1. Magnetron Sputtering

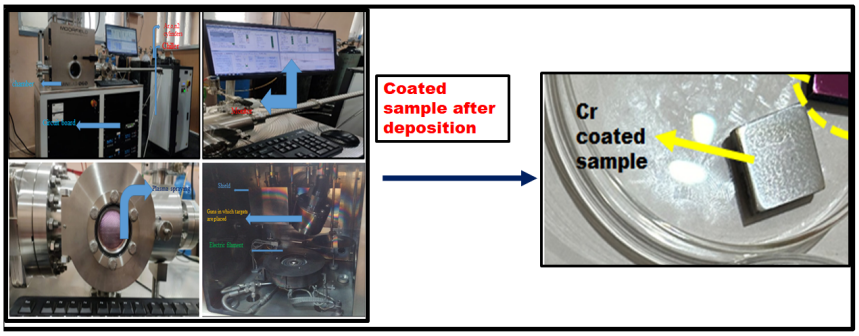

Figure 2: Shows A Systematic View of Magnetron Sputtering Machine with Coated Sample

2.2. Nano Indenter

The Nano indenter Hysteron TI Premier was used for Nano indentation testing. Different loads ranging from 200µN to 1000 µN were used to take indents on these loads. Berkovich indenter was used in the indentation process. Furthermore, the same load analysis was performed on chromium coated and bare substrate samples. The tests were performed for samples at a temperature of 100°C. This further helped calculate hardness and Modulus of elasticity at different temperatures.

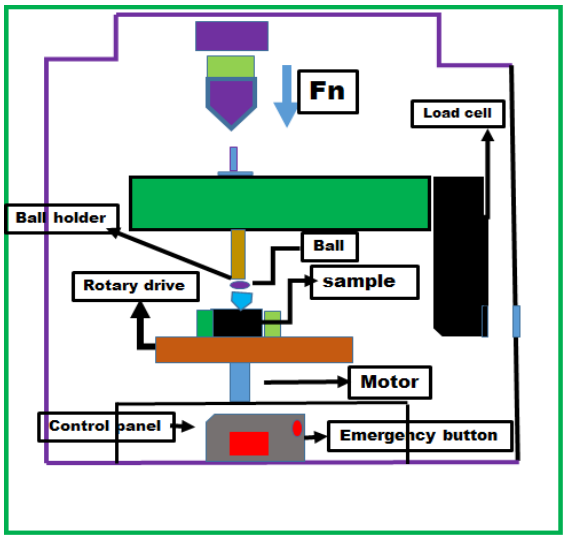

Figure 3: Systematic View of Nano Indentation of Machine

Target	**I.Chromium (99% pure and 58.5 mm diameter and 5mm thickness)**
Base pressure in bar	3.66×10^{-7}
Deposition gas pressure (Ar)/bar	5.32×10^{-6}
Base pressure for Cr	3.33×10^{-7}
Deposition power/W	100 W for chromium target,
Deposition time for Cr coating/min	60 minutes
Substrate	Superni-718
Substrate temperature/ ℃	**100**
Total Deposition time/min	**60 minutes**

Table 3: Process Parameters for Deposition of Chromium on Magnetron Sputtering

2.3. Characterization

XRD and FE-SEM/EDS were used to analyse the mechanical characterization of coated and uncoated samples. SEM-EDS was used to analyse the cross-section of the coated sample.

2.4. Nano Indentation

The Nano indentation was performed on bare and coated samples using the Berkovich indenter. The Nano indentation was performed on five different loads ranging from200µN to 1000µN load. AFM observed the indent depth, and the hardness modulus of elasticity was calculated using the Oliver and Pharr model.

3. Results and Discussions

3.1. Surface Morphology of Substrate and Coated Chromium Sample

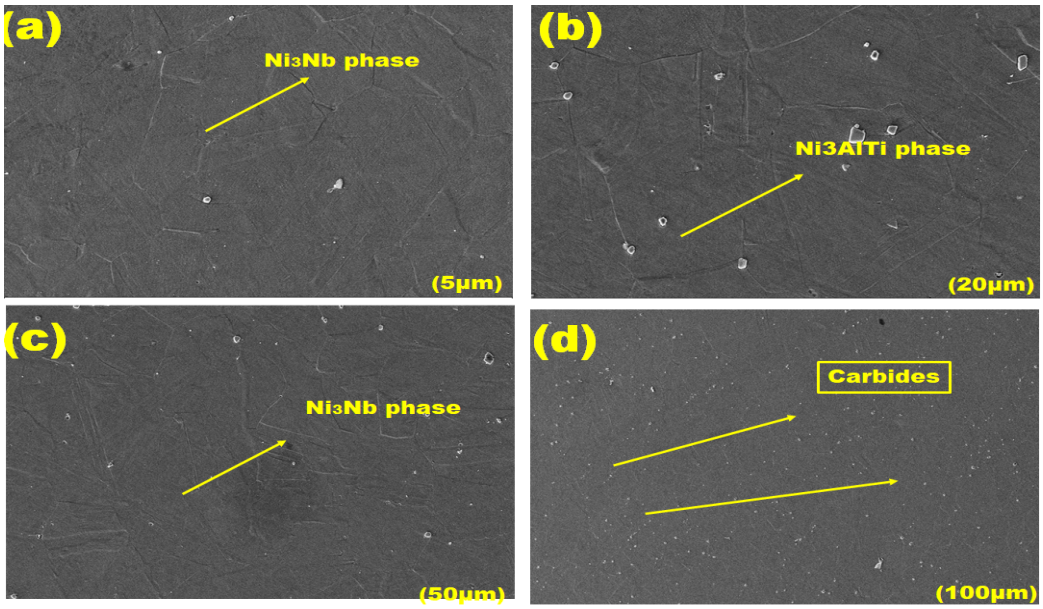

Figure 4: FESEM Images of Inconel Substrate

Figure 4 shows the surface is less detailed than in the upper left FESEM image, but it still contains some noticeable pits and depressions. The texture is generally less rough but still uneven, with a few apparent places that might be pores, pits, or some other material fault. A 2µm scale was used to measure the graph. The surface is less detailed than in the upper left FESEM image but still contains some noticeable pits and depressions. The texture is generally less rough but still uneven, with a few apparent places that might be pores, pits, or some other material fault. This picture displays a smoother surface with less apparent particle debris or roughness. The image shows more extensive surface details, which tends to prioritise overall morphology over specific features. The measurement scale for this graph is 5 µm. The surface exhibits a delicate, granular texture at this very high magnification. The FESEM image most likely shows the material's microstructure, with its tiny particles or features. A few flaws or inclusions could appear as darker patches. These micrographs were taken of a material at various scales from its surface to study its shape, texture, and possible defects. Each image's many magnification levels help to understand the material surface properties and faults.

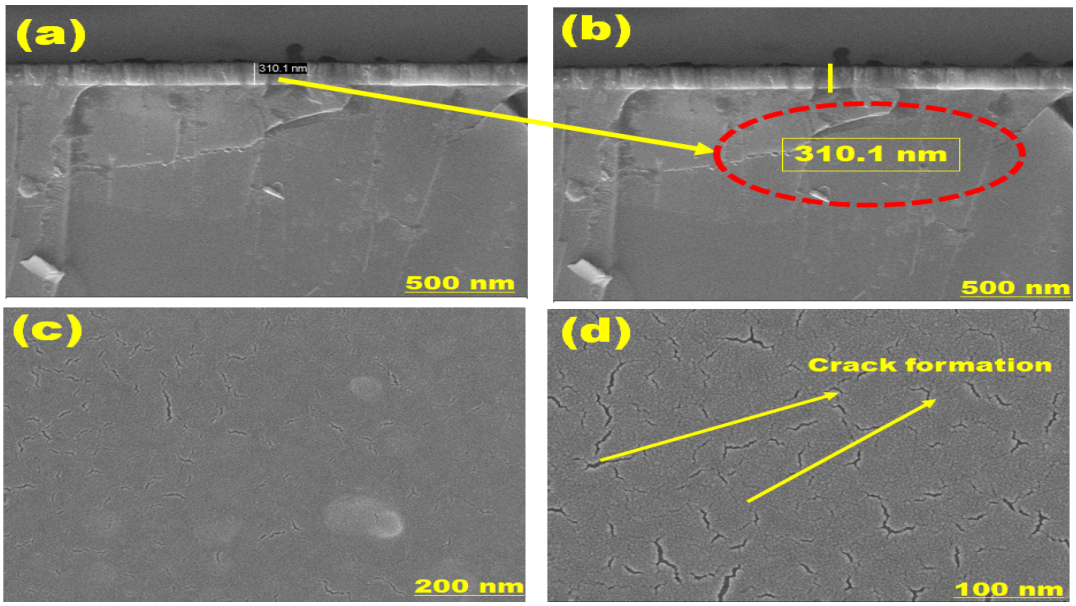

Figure 5: FESEM Images of Chromium Coated Sample

Figure 5-a shows the chromium layer deposited on the super-718 substrate for one hour of deposition. The thickness obtained after one hour of deposition is 310 nm, and the coating is columnar structured in nature. Figure 5-b shows the microstructure of chromium coating deposited on super ni 718.The figure 5c and 5d shows the microstructure of chromium coating that is deposited for one hour the microstructure shows crack formation as the coating has been deposited on substrate on DC power. The coating deposited seems to be porous as it is deposited at a substrate temperature of 100°C, and the FESEM images of the chromium-coated sample reveal a beautifully even layer of Chromium, meticulously applied with a thickness of 310 nm. This precise thickness showcases the high level of control during the coating process, ensuring a smooth, uniform surface. At a closer look, the chromium coating appears flawless, soft and dense, without noticeable imperfections. The cross-sectional images highlight the sharp boundary between the Chromium and the substrate, a testament to the quality and consistency of the application. This 310 nm chromium layer is deposited to shield the material beneath from wear and corrosion, making it resilient in harsh conditions.

3.2. XRD Analysis

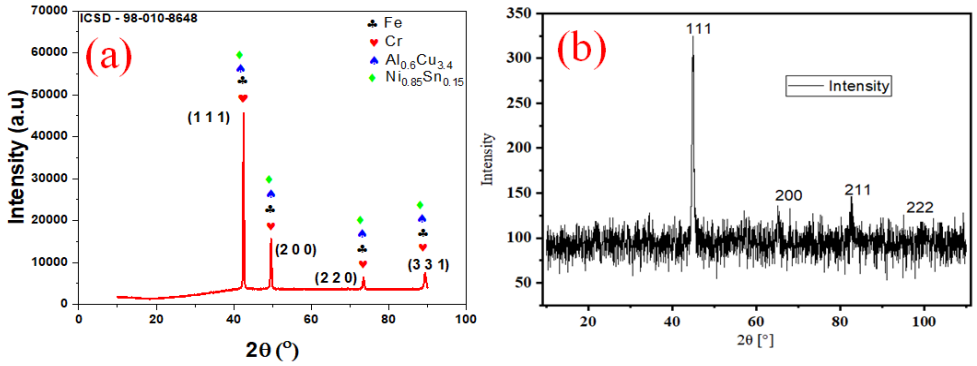

Figure 6: XRD Analysis of Chromium Coated Sample and Bare Sample

Figure 6-a shows Low Angles (20° to 40°) and broad peaks are caused by macrostrain effects or smaller crystallite sizes. Furthermore, this region may suggest the presence of subsequent phases, such as carbides. Prominent γ matrix peaks predominate between 40° and 70°, which are mid-angle angles. Peak movements in this region could indicate lattice strain or compositional changes. High Angles 70° - 90°, weaker peaks are often observed here, but they can provide more insight into the phase's composition and any lesser phases. Figure 6-b shows additional peaks corresponding to the Chromium (Cr) bond coating, which will appear in the coated sample's XRD pattern. For chromium (body cantered cubic BCC structure), the (110), (200), and (211) planes usually display the most noticeable peaks. Oxide phases such as chromium oxides (Cr2O3) may also be found, depending on the

deposition conditions. In a sample without a coating, as shown in figure 6-a, the peaks on the substrate represent the grain size of the bulk material, which is often significantly more extensive than that of nanostructured coatings, and because of the finer grain size (nanometre scale), the peaks for the nanostructured chromium coating are typically larger as shown in figure 6-b

3.3. EDS Analysis

In order to reveal the chemical composition and elemental distribution the EDS was performed on substrate as well as on chromium coated sample

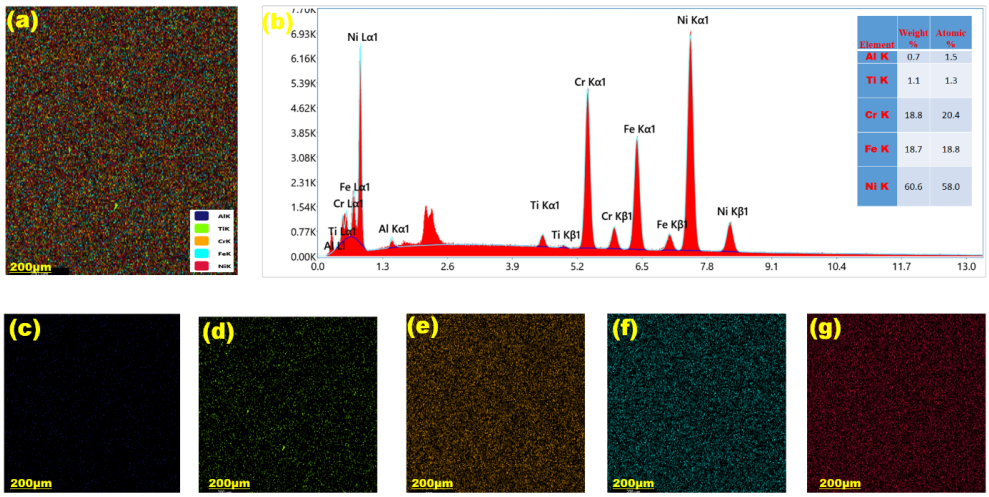

Figure 7: Shows the EDS Of the Substrate

Figure 7-a shows the EDS images behind the overlay, providing maps of the elements Al, Ti, Cr, Fe, and Ni in various colours, signifying their spatial distribution and presence throughout the region. These maps show which areas of the sample have more significant amounts of each element, and the weight percentage of each component are shown in the table: Ni (60.6%), Cr (18.5%), Fe (18.7%), Ti (1.1%), and Al (0.7%). This information offers a numerical evaluation of sample composition. The existence of each element is confirmed by peaks in the EDS spectrum that correspond to specific energies (e.g., Ni, Cr, and Fe). According to the table data, Ni exhibits distinct peaks, with each peak height and size indicating the relative concentration of each element

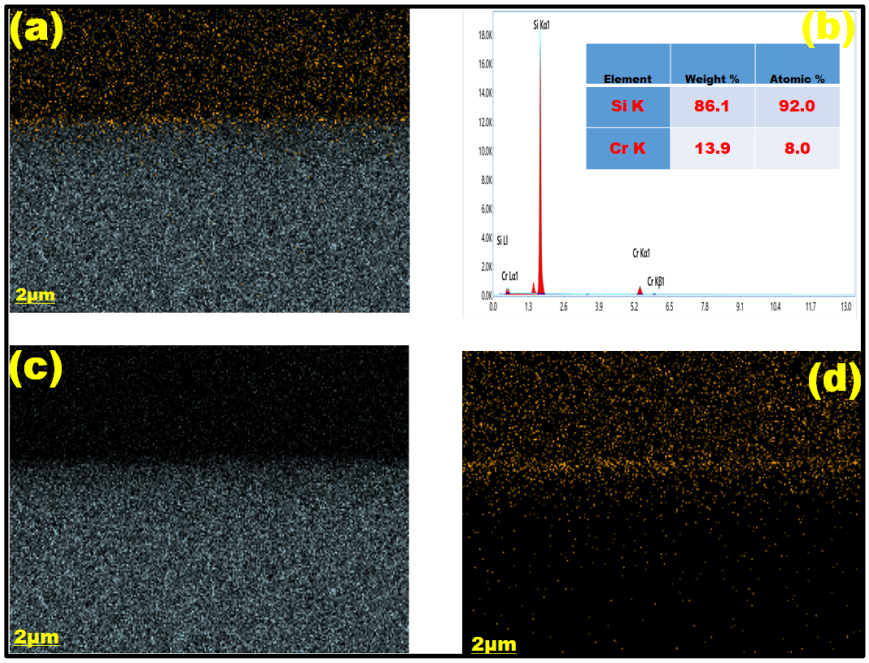

Figure 8: Show EDS Of Chromium Coated Sample.

In Figure 8-a, a secondary electron or backscatter image displaying structural or compositional contrast, with distinct regions marked by a considerable border and elemental map showing the distribution of a Cr element. The table in Figure 8-b shows Si and Cr atomic and weight percentages. The silicon wafer's atomic percentage is 86.1% (92.0% by weight), while Cr is 13.9% (8.0% by weight) since Chromium is deposited on a silicon wafer so that is why it is showing elemental composition of silicon.

3.4. Nano Mechanical Characterizations

S.no	Modulus of elasticity for Chromium (E) Gpa	Relative Modulus of elasticity for Chromium (Er) Gpa	Hardness value for Chromium (H)	Load (µN)	Contact Depth (nm)
1	512	95.36	7.40	200	31.66
2	304	85.31	6.41	400	41.22
3	199	74.92	5.52	600	53.21
4	159.639	69.14	5.05	800	63.99
5	147.73	67.93	5	1000	77.3

Table 4: Calculation of The Value of Hardness and Modulus of Elasticity for Chromium Coating

Information about Inconel 718 performance qualities can be gleaned from examining its mechanical properties under various loads. Although Inconel 718 has exceptional mechanical attributes, it also displays behaviour typical of ductile materials under increased stress, as evidenced by the notable fluctuation in Modulus of elasticity, hardness, and contact depth with applied load. Future research should assess Inconel 718 long-term performance under actual application circumstances, such as high-temperature settings, to guarantee dependability and performance.

S.no	Modulus of elasticity for Inconel -718(E) Gpa	Relative Modulus of elasticity for Inconel -718 (Er) Gpa	Hardness value for Inconel -718 (H)	Load (µN)	Contact Depth (nm)
1	400	90.35	4.39	200	33
2	150	68.42	3.05	400	62.3
3	140	67.42	3	600	79.2
4	112	59.02	2.57	800	102
5	107	58.66	2.45	1000	115.3

Table 5: Calculation of The Value of Hardness and Modulus of Elasticity for Inconel-718

$$\frac{1}{Er} = \frac{1-\nu^2}{E} + \frac{1-\nu i^2}{Ei} \qquad (1)$$

Where E is the elastic Modulus of the coating.
ν is the poison ratio of the test material
Ei elastic modulus of indenter Ei =1141 GPa
νi is the poison ratio indenter νi = 0.07

The above equation is used to calculate the hardness and Modulus of elasticity, and this equation is based on the Oliver and Pharr model.

The findings in Table 5 show that Chromium has good mechanical qualities at first but becomes more prone to wear and distortion when loads increase. A change from elastic to plastic behaviour is suggested by decreasing Modulus and hardness under loading circumstances. Significant changes in the Modulus of elasticity, hardness, and contact depth with increasing stress are revealed by examining the mechanical characteristics of chromium coatings under various loads. Although chromium coatings offer superior mechanical performance initially, their vulnerability to distortion at higher loads calls for cautious application planning. Table 5 shows results structured on different loads for each coating. The Modulus of elasticity and value of hardness have been calculated on each load ranging from 200-1000µN.

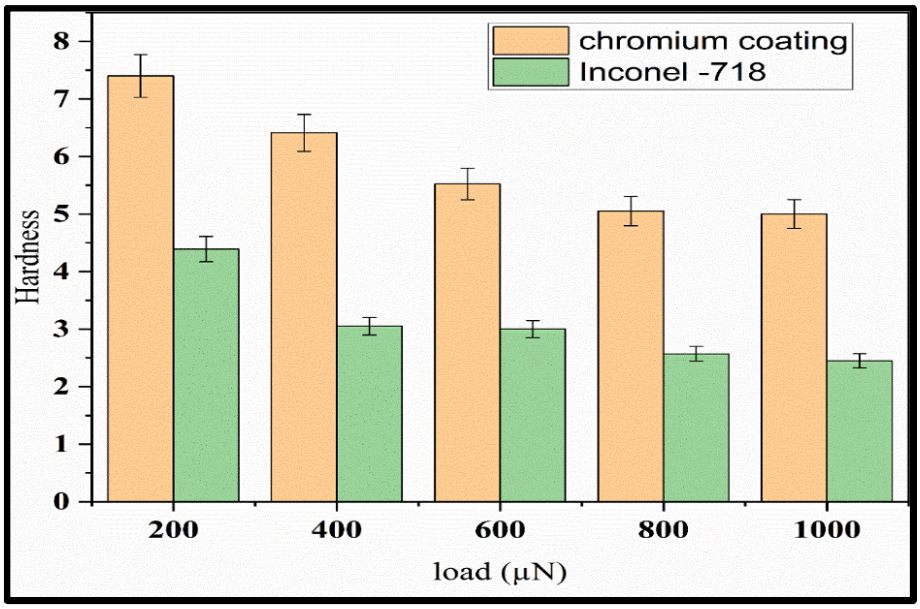

Figure 9: Hardness of Substrate and Chromium Coated Sample

Figure 9 shows the hardness value on different loads, for coated as well as on substrate on various loads. The figure clearly indicates that the value of hardness is enhanced with chromium coating compared with the uncoated sample.

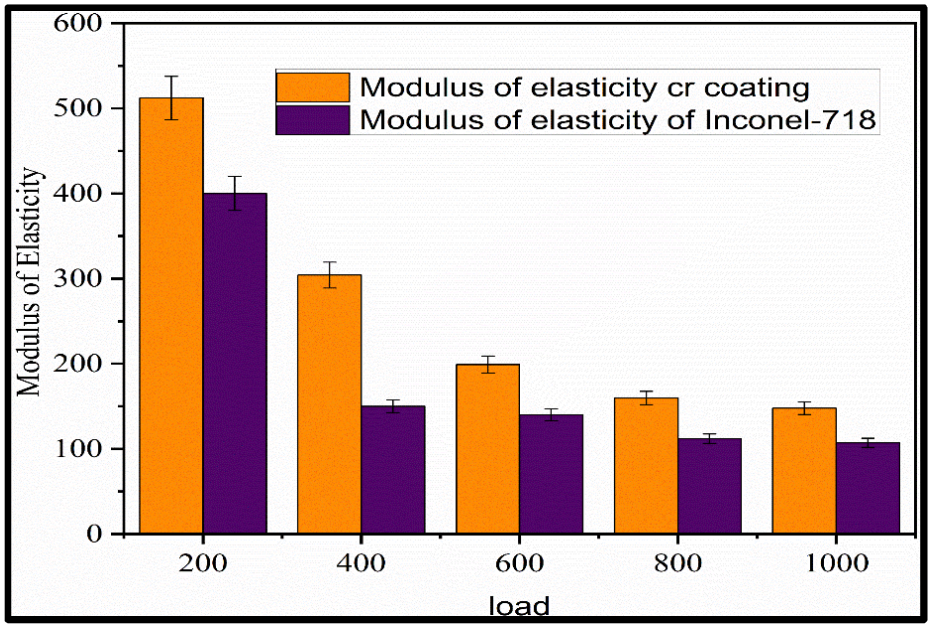

Figure 10: Calculation of Modulus of Elasticity for Chromium Coating and Inconel -718

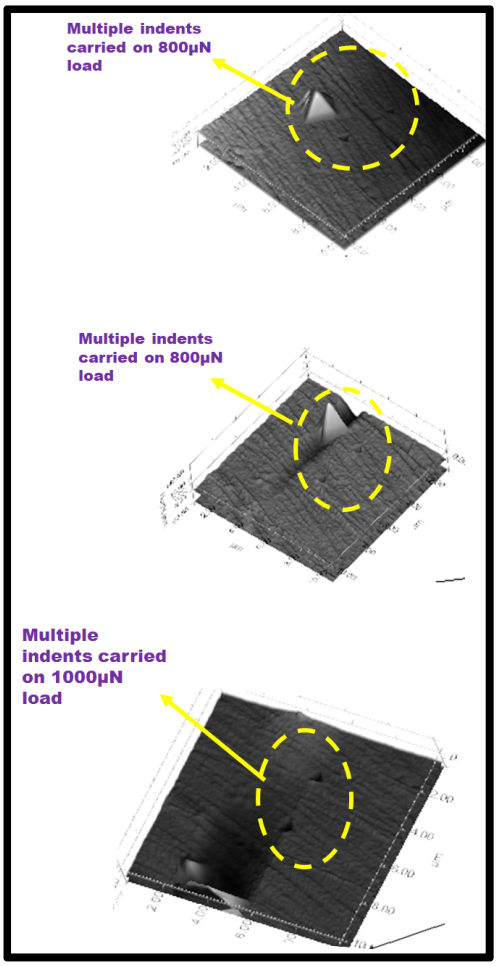

Figure 11: AFM Images of Indents Performed on The Substrate and Coated Sample

The Nano indentation was carried on different loads and multiple indents were carried out on each load as is how in AFM images in figure 11 and value of hardness was carried out by taking the aggregate mean of all the indents performed on particular load. Figure 11 are the AFM images of different indents performed on different loads on substrate ranging from 600µN to 1000µN load, and these are marked in yellow colour are the indents performed on Chromium coated sample. Indentation experiments were carried out on chromium coatings at five distinct load levels, from 200 µN to 1000 µN, with results on depth of indent, hardness, and elastic Modulus organized in a table. Atomic Force Microscopy (AFM) images provided insights into how the hardness and elasticity of the chromium coating respond to different loads. As the load increased, the indentation depth and corresponding deformation were closely analysed to understand how the coating reacts under mechanical stress

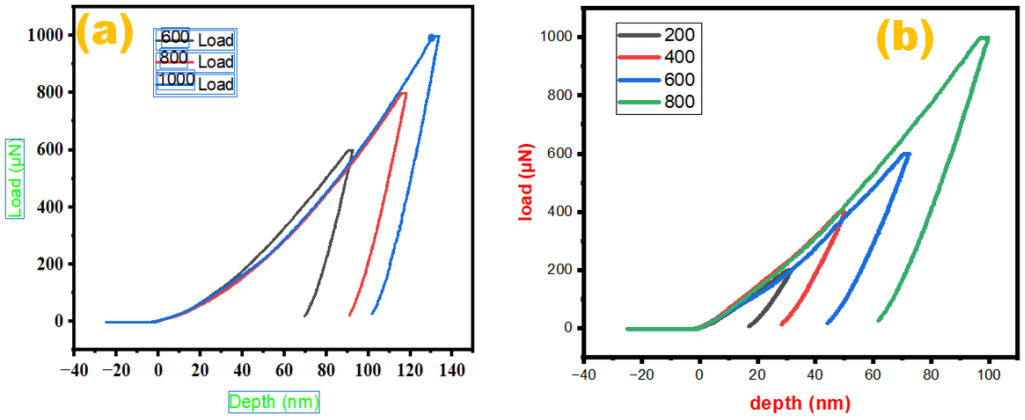

Figure 12: Load Vs Depth of Substrate and Chromium-Coated Sample

Figure 12-a shows the depth of the indenter with load, and it can be seen from Figure 12-b that the depth of the indenter is less with the same applied load, thus it clearly shows the impact of coating on the overall hardness; the load versus depth analysis for both the substrate and the Chromium coated sample provides valuable insights into the mechanical behaviour of each under load. As load is applied, the indentation depth increases, revealing differences in how the substrate and the coated sample handle stress. The substrate alone shows a relatively greater indentation depth under the same load compared to the chromium-coated sample, indicating that the chromium layer adds hardness and resistance to deformation. This added layer is a protective shield, reducing the indentation depth and thus better preserving the underlying material. At lower loads, both the substrate and the coated sample exhibit minimal indentation. Still, as the load increases, the coated sample's resistance becomes more apparent, with the coating distributing the pressure more effectively. The chromium coating improves the surface hardness and enhances the material ability to withstand higher loads without significant deformation. This study emphasizes how a well applied chromium coating can prolong the life of the substrate by protecting it against deep indentations and mechanical wear, making it more durable in demanding applications.

3.5. Nano Scratch

Nano scratch is used to check the adhesion strength of coating substrate system .Three Nano scratch of 6 mm in length were performed on coating surface using diamond shaped Nano indenter and loads were varied up to 2000µN and the three different modes of failure were observed ,the load at which coating fails is called as critical load [36]. A Rockwell C diamond tip (200 µm radius) was drawn over the coated surface for 6 mm length as the applied normal load increased continuously up to 2000 µN. The diamond tip was cleaned after each scratch and the test was repeated twice on each sample. For Cr coatings, 3 scratch tests were performed with an increasing normal load value up to 2000 µN in a 6 mm length line. Acoustic emissions were recorded during the scratching.

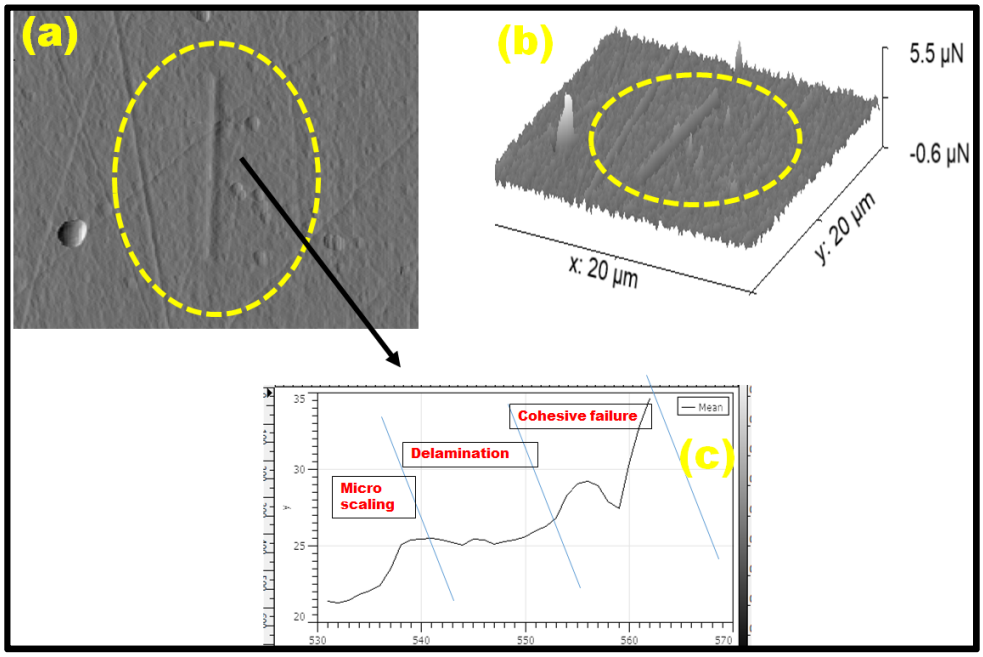

Figure 13: Nano Scratch Performed on Chromium Coated Sample At 2000µN Load

Generally, three modes of failure mechanism are obtained from Nano scratch analysis [37]

Lc_1: micro scaling.

Lc_2: delamination.

Lc_3: cohesive failure mode.

Since coating is only 310 nm still coating substrate system has shown good adhesion strength.

4. Conclusion

- 1 Evaluated the mechanical behaviour of chromium coatings on Superni-718 at 100 °C.
- Significant improvements in hardness, compared to uncoated Superni-718 there has been significant improvement in hardness as much as 52% increase on every load and modulus of elasticity enhanced to 21% on different loads.
- Cr Coating has a superior modulus of elasticity compared to Inconel-718 across all load conditions. At lower loads, the difference is much more pronounced, making Cr coating a better choice for applications requiring higher rigidity and less deformation [38].
- Uniformly dense structure with remarkable mechanical properties and thickness achieved on 310 nm coating thickness.
- The microstructural analysis revealed that after depositing chromium coating on superni -718 revealed columnar

structure and coating deposited was dense while as substrate simply showed phases that are in substrate.

- Nano scratch revealed better adhesion and less delamination failure of chromium coating.

References

1. Wu, S. (2022). Development of additively manufactured nickel-based superalloys toward optimal creep performance. *PhD diss., Monash University.*
2. Singh, R., & Sharma, V. (2022). Machining induced surface integrity behavior of nickel-based superalloy: effect of lubricating environments. *Journal of Materials Processing Technology, 307*, 117701.
3. Sáenz-Trevizo, A., & Hodge, A. M. (2020). Nanomaterials by design: a review of nanoscale metallic multilayers. *Nanotechnology, 31*(29), 292002.
4. Nair, A., Kumanan, S., Prakash, C., Mohan, D. G., Saxena, K. K., Kumar, S., & Kumar, G. (2023). Research developments and technological advancements in conventional and non-conventional machining of superalloys–a review. *Journal of Adhesion Science and Technology, 37*(22), 3053-3124.
5. Khanna, A. S., & Jha, S. K. (1998). Degradation of materials under hot corrosion conditions. *Transactions of the Indian Institute of Metals, 51*(5), 279-290.
6. Kaur, M., Singh, H., & Prakash, S. (2009). High-temperature corrosion studies of HVOF-sprayed Cr3C2-NiCr coating on SAE-347H boiler steel. *Journal of thermal spray technology, 18*(4), 619-632.
7. Kaur, M., Singh, H., & Prakash, S. (2011). Surface engineering analysis of detonation-gun sprayed Cr3C2–NiCr coating under high-temperature oxidation and oxidation–erosion environments. *Surface and Coatings Technology, 206*(2-3), 530-541.
8. Sidhu, B. S., & Prakash, S. (2006). Erosion-corrosion of plasma as sprayed and laser remelted Stellite-6 coatings in a coal fired boiler. *Wear, 260*(9-10), 1035-1044.
9. Chawla, V., Chawla, A., Puri, D., Prakash, S., & Sidhu, B. S. (2011). Performance of nanostructured metal nitride coated T-22 boiler steel in Na 2 SO 4–60% V 2 O 5 Environment at 900 C under cyclic conditions. *Journal of Minerals and Materials Characterization and Engineering, 10*(07), 583.
10. Sidhu, B. S., Puri, D., & Prakash, S. (2004). Characterisations of plasma sprayed and laser remelted NiCrAlY bond coats and Ni3Al coatings on boiler tube steels. *Materials Science and Engineering: A, 368*(1-2), 149-158.
11. Pawlowski, L. (2008). *The science and engineering of thermal spray coatings*. John Wiley & Sons.
12. Hay, J., & Crawford, B. (2011). Measuring substrate-independent modulus of thin films. *Journal of Materials Research, 26*(6), 727-738.
13. Oliver, W. C., & Pharr, G. M. (1992). An improved technique for determining hardness and elastic modulus using load and displacement sensing indentation experiments. *Journal of materials research, 7*(6), 1564-1583.
14. Doerner, M. F., & Nix, W. D. (1986). A method for interpreting the data from depth-sensing indentation instruments. *Journal of Materials research, 1*(4), 601-609.
15. Huajian, G., Cheng-Hsin, C., & Jin, L. (1992). Elastic contact versus indentation modeling of multi-layered materials. *International journal of Solids and Structures, 29*(20), 2471-2492.
16. Sibin, K. P., John, S., & Barshilia, H. C. (2015). Control of thermal emittance of stainless steel using sputtered tungsten thin films for solar thermal power applications. *Solar energy materials and solar cells, 133*, 1-7.
17. Shield, T. W., & Bogy, D. B. (1989). Some axisymmetric problems for layered elastic media: Part I—Multiple region contact solutions for simply-connected indenters.
18. Seshan, K. (2002). *Handbook of thin film deposition techniques principles, methods, equipment and applications, second editon*. CRC press.
19. Barna, P. B., & Adamik, M. J. T. S. F. (1998). Fundamental structure forming phenomena of polycrystalline films and the structure zone models. *Thin solid films, 317*(1-2), 27-33.
20. Bermejo, R., Sanchez-Herencia, A. J., Baudin, C., & Llanes, L. (2006). Residual stresses in Al2O3-ZrO2 multilayered ceramics: nature, evaluation and influence on the structural integrity. *Boletin de la sociedad Espanola de Ceramica y Vidrio, 45*(5), 352-357.
21. Luu, H. T., Raumel, S., Dencker, F., Wurz, M., & Merkert, N. (2022). Nanoindentation in alumina coated Al: molecular dynamics simulations and experiments. *Surface and Coatings Technology, 437*, 128342.
22. Jahanshahi, M., Mofidian, R., Hosseini, S. S., & Miansari, M. (2023). Investigation of mechanical properties of granular γ-alumina using experimental nano indentation and nano scratch tests. *SN Applied Sciences, 5*(6), 164.
23. King, R. B. (1987). Elastic analysis of some punch problems for a layered medium. *International Journal of Solids and Structures, 23*(12), 1657-1664.
24. Garton, D. B. (2011). Vacuum technology and vacuum design handbook for accelerator technicians.
25. Bosco, R., Van Den Beucken, J., Leeuwenburgh, S., & Jansen, J. (2012). Surface engineering for bone implants: a trend from passive to active surfaces. *Coatings, 2*(3), 95-119.
26. Grovenor, C. R. M., Hentzell, H. T. G., & Smith, D. A. (1984). The development of grain structure during growth of metallic films. *Acta Metallurgica, 32*(5), 773-781.
27. Mishra, S. K., Rupa, P. K. P., & Pathak, L. C. (2007). Surface and nanoindentation studies on nanocrystalline titanium diboride thin film deposited by magnetron sputtering. *Thin Solid Films, 515*(17), 6884-6889.
28. Sanchez, C. M. T., Plata, B. R., da Costa, M. M., & Freire Jr, F. L. (2011). Titanium diboride thin films produced by dc-magnetron sputtering: Structural and mechanical properties. *Surface and Coatings Technology, 205*(12), 3698-3702.
29. Dai, W., Zhang, T., Yang, J., Sun, R., & Xu, J. (2008). Morphological analysis of TiB2 thin film prepared by rf magnetron sputtering. *Journal of Vacuum Science & Technology A, 26*(4), 610-615.
30. Psiuk, R., Milczarek, M., Jenczyk, P., Denis, P., Jarząbek,

D. M., Bazarnik, P., ... & Mościcki, T. (2021). Improved mechanical properties of W-Zr-B coatings deposited by hybrid RF magnetron–PLD method. *Applied Surface Science, 570*, 151239.

31. Bakhit, B., Petrov, I., Greene, J. E., Hultman, L., Rosén, J., & Greczynski, G. (2018). Controlling the B/Ti ratio of TiBx thin films grown by high-power impulse magnetron sputtering. *Journal of Vacuum Science & Technology A, 36*(3).
32. Thörnberg, J., Palisaitis, J., Hellgren, N., Klimashin, F. F., Ghafoor, N., Zhirkov, I., ... & Rosen, J. (2020). Microstructure and materials properties of understoichiometric TiBx thin films grown by HiPIMS. *Surface and Coatings Technology, 404*, 126537.
33. Palisaitis, J., Dahlqvist, M., Hall, A. J., Thörnberg, J., Persson, I., Nedfors, N., ... & Persson, P. O. (2021). Where is the unpaired transition metal in substoichiometric diboride line compounds?. *Acta Materialia, 204*, 116510.
34. Nedfors, N., Mockute, A., Palisaitis, J., Persson, P. O., Näslund, L. Å., & Rosen, J. (2016). Influence of pulse frequency and bias on microstructure and mechanical properties of TiB2 coatings deposited by high power impulse magnetron sputtering. *Surface and Coatings Technology, 304*, 203-210.
35. Thörnberg, J., Bakhit, B., Palisaitis, J., Hellgren, N., Hultman, L., Greczynski, G., ... & Rosen, J. (2021). Improved oxidation properties from a reduced B content in sputter-deposited TiBx thin films. *Surface and Coatings Technology, 420*, 127353.
36. Wolfe, D. E., Singh, J., & Narasimhan, K. (2003). Synthesis and characterization of multilayered TiC/TiB2 coatings deposited by ion beam assisted, electron beam–physical vapor deposition (EB–PVD). *Surface and Coatings Technology, 165*(1), 8-25.
37. Guo, F., Zhou, R., Shang, Y., Zhang, H., Pei, Y., Li, S., & Gong, S. (2021). Development of deposition beam current dependent microstructure and nanomechanical properties in ZrO2-8wt% Y2O3 thermal barrier coatings produced by electron beam-physical vapor deposition technique. *Materials Chemistry and Physics, 272*, 124998.
38. Kadam, N. R., Karthikeyan, G., & Kulkarni, D. M. (2020). Effect of substrate rotation on the microstructure of 8YSZ thermal barrier coatings by EB-PVD. *Materials Today: Proceedings, 28*, 678-683.
39. Wada, K., Yamaguchi, N., & Matsubara, H. (2005). Effect of substrate rotation on texture evolution in ZrO2-4 mol.% Y2O3 layers fabricated by EB-PVD. *Surface and coatings technology, 191*(2-3), 367-374.
40. Bull, S. J., & Berasetegui, E. G. (2006). An overview of the potential of quantitative coating adhesion measurement by scratch testing. *Tribology International, 39*(2), 99-114.
41. Lukaszkowicz, K., Kriz, A., & Sondor, J. (2011). Structure and adhesion of thin coatings deposited by PVD technology on the X6CrNiMoTi17-12-2 and X40 CrMoV5-1 steel substrates. *Archives of Materials Science and Engineering, 51*(1), 40-47.
42. Yang, Z., Zhang, N., Li, H., Chen, B., & Yang, B. (2023). Comparison to micro wear mechanism of PVD chromium coatings and electroplated hard chromium. *Materials, 16*(7), 2695.